Pertanika J. Sci. & Technol. 32 (6): 2561 - 2574 (2024)

PERTANIKA JOURNALS

SCIENCE & TECHNOLOGY

Journal homepage: http://www.pertanika.upm.edu.my/

Low-temperature Deposited Highly Sensitive Integrated All-Solid Electrodes for Electrochemical pH Detection

Norhidayatul Hikmee Mahzan[1,2], Shaiful Bakhtiar Hashim[1,2], Rosalena Irma Alip[2]*, Zuhani Ismail Khan[3] and Sukreen Hana Herman[2,3]

[1]Nano-Electronic Center (NET), School of Electrical Engineering, College of Engineering, Universiti Teknologi MARA, 40450 Shah Alam, Selangor, Malaysia

[2]Integrated Sensors Research Group, School of Electrical Engineering, College of Engineering, Universiti Teknologi MARA, 40450 Shah Alam, Selangor, Malaysia

[3]Microwave Research Institute, Universiti Teknologi MARA, 40450 Shah Alam, Selangor, Malaysia

ABSTRACT

This article describes the process of fabricating an integrated all-solid electrode (IASE) by integrating thin films of titanium dioxide (TiO_2) and silver/silver chloride (Ag/AgCl) onto an indium tin oxide (ITO) substrate. The fabrication of a pH sensing electrode (SE) involved utilizing a spin-coated thin film composed of TiO_2. Thermally produced thin films of Ag/AgCl were used to develop solid reference electrodes (RE). The present work examined the impact of the drying process on the pH sensitivity and linearity of the low-temperature deposited IASE. The drying procedure was carried out within a temperature range from room temperature to 100°C. The investigation involved the examination of crystallinity, surface morphology, and thin film composition through the utilization of field effect scanning electron microscopy (FESEM), X-ray diffraction (XRD), and energy-dispersive X-ray (EDX) methods. In addition, a comparison was made between the pH sensing performance of the IASE and a commercially available Ag/AgCl RE. The findings of this research demonstrate that the IASE sample, which underwent a drying process at a temperature of 100°C, exhibited remarkable sensitivity and linearity values of 66.7 mV/pH and 0.9827, separately, when compared to the commercially available RE.

ARTICLE INFO

Article history:
Received: 11 December 2023
Accepted: 10 June 2024
Published: 25 October 2024

DOI: https://doi.org/10.47836/pjst.32.6.08

E-mail addresses:
hikmee@uitm.edu.my (Norhidayatul Hikmee Mahzan)
shaifulbakhtiar@uitm.edu.my (Shaiful Bakhtiar Hashim)
rosalena@uitm.edu.my (Rosalena Irma Alip)
zuhai629@uitm.edu.my (Zuhani Ismail Khan)
hana1617@uitm.edu.my (Sukreen Hana Herman)
*Corresponding author

Keywords: Integrated-all solid electrodes, pH sensor; reference electrodes, sensing electrodes, titanium dioxide

ISSN: 0128-7680
e-ISSN: 2231-8526

INTRODUCTION

pH is an essential parameter in various fields, including agriculture (Gao et al., 2022; He et al., 2022), medical applications (Chalitangkoon & Monvisade, 2021), and food processing (Fathi et al., 2022; Zou et al., 2023). The ability to determine the level of acidity or alkalinity in a solution is significantly influenced by the pH value. The conventional method of pH measurement involves using glass electrodes, which have gained widespread popularity. However, the fragility of glass-based electrodes limits their utility and hinders their miniaturization for certain applications, particularly in the medical field (Manjakkal et al., 2020). Additionally, the maintenance of such pH sensors is labor-intensive due to the requirement of an internal solution, typically saturated potassium chloride (KCl). Consequently, there is a need for alternative pH sensing approaches that offer improved durability and reduced maintenance.

In 1972, P. Bergveld introduced a novel solid-state pH sensor, the ion-sensitive field effect transistor (ISFET), in response to the challenges associated with glass electrode fragility and maintenance requirements (Bergveld, 1972). The utilization of ISFETs enabled the quantification of ionic reactions occurring in electrochemical and biological surroundings. Nevertheless, certain drawbacks were discovered upon its implementation, particularly in relation to temperature sensitivity, susceptibility to light interference, and ionic penetration issues. To address these challenges, Spiegel proposed an alternative solution in 1983: the extended gate field effect transistor (EGFET) detection method (Spiegel et al., 1983). The EGFET pH sensor offered several notable advantages over the ISFET, including enhanced stability in varying light and temperature conditions, heightened sensitivity, reduced impedance, cost-effectiveness, and simplified packaging (Mokhtarifar et al., 2018; Pullano et al., 2018).

Various metal oxides, including tantalum oxide (Ta_2O_5), zinc oxide (ZnO), copper oxide (CuO), tin oxide (SnO_2) and titanium dioxide (TiO_2) have found widespread applications in diverse fields (Beale et al., 2022; Khizir & Abbas, 2022; Palit et al., 2020; Ramakrishnappa et al., 2020; Sharma & Kumar, 2022). Among these metal oxides, TiO_2 has emerged as a highly promising material, demonstrating significant potential in various applications such as memristors, dye-sensitized solar cells, photocatalysts, capacitors, gas sensors, pH-sensing electrodes (SE) and tailoring the charge storage properties (Krishnan et al., 2016; Özdemir et al., 2022; Pal et al., 2018; Sadig et al., 2019; Tayeb et al., 2022; Zamiri et al., 2022; Zulkefle et al., 2021). When employed as a SE, TiO_2 offers exceptional attributes, including excellent chemical stability, flexibility, robustness, and a high dielectric constant. Several fabrication techniques for TiO_2 SE have been documented, including sputtering, spin coating, physical and chemical vapor deposition, immersion techniques, spray pyrolysis, electron beam deposition, and pulsed laser deposition (Dave & Chauhan, 2022; Radha et al., 2022; Song et al., 2023; Yang et al., 2023). The sol-gel spin coat process is the simplest

and least expensive of these options. It makes it easier for chemicals to react evenly with the thin films and the substrate, especially when the temperatures are high.

The primary aim of this investigation is to examine the performance of sensitivity for integrated all-solid electrodes (IASE) through the application of a TiO_2 SE and an Ag/AgCl reference electrode (RE) onto a singular indium tin oxide (ITO) substrate. It is hypothesized that utilizing TiO_2 as the SE and Ag/AgCl as the RE will result in enhanced durability, potential for downsizing, and reduced maintenance demands compared to conventional glass-based pH sensors. In this study, we analyzed the operational efficiency of the developed IASE system and compared it to a TiO_2 SE paired with a commercially available RE. The present studies are anticipated to provide an important and useful addition to the advancement of pH sensing devices that are both efficient and dependable, hence enhancing their applicability across several domains.

MATERIALS AND METHODS

Sample Preparations

The IASE was fabricated by constructing an SE and a RE on a single ITO-coated glass substrate. Figure 1 shows the top view configuration of the IASE, with the Ag/AgCl RE and TiO_2 SE occupying an area of 0.35 cm^2 and being separated by 0.6 cm^2 of the insulation region. The insulation region was created by removing the conductive ITO coating using zinc powder and hydrochloric acid (HCl). This removal was crucial to prevent electrical linkage between the SE and the RE.

Prior to fabricating the IASE, the ITO substrate underwent ultrasonic cleaning using Hwashin Technology Powersonic 405. The substrate was cleaned by submerging it for ten minutes at a time in a solution of ethanol and deionized water and then drying it with inert nitrogen gas.

To produce TiO_2, a solution containing mixtures A and B was combined. Mixture A comprised absolute ethanol as a solvent, glacial acetic acid as a stabilizer, and titanium (IV) isopropoxide as the precursor. In contrast, mixture B consists of deionized water, Triton X-100 utilized as a surfactant and absolute ethanol. Both mixtures were organized separately, each undergoing a one-hour stirring process. Subsequently, the mixtures were combined and subjected to an additional hour of stirring at room temperature.

The sol-gel spin coater (Laurell Model WS-650MZ-8NPP/LITE) was used to deposit a thin film of TiO_2 from the TiO_2 solution that had been prepared. This spin-coating method has been recognized to yield uniform thin films. The deposition process was initiated by carefully positioning the cleaned ITO substrate onto the spin coater's chuck and dispensing 10 drops of TiO_2 solution onto the substrate. Initially, the substrate was rotated at 500 rpm for 10 seconds, after which the rotational speed was increased to 3000 rpm for one minute. High-speed spinning evenly dispersed the solution across the substrate surface, creating

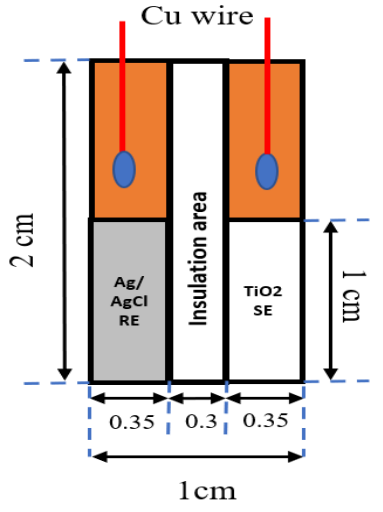

Figure 1. IASE top view configuration

a thin coating with consistent thickness. After that, the film was dried at 100°C for 10 minutes to remove any remaining solvents, including ethanol and water, thus leaving behind a pure TiO_2 thin film. A single layer of TiO_2 thin film with an approximate thickness of 23 nm was produced on the substrate by annealing the sample for 15 minutes at 400°C after drying it.

A thermal evaporator (TE) was employed to deposit the Ag layer, a commonly utilized thin metal film deposition method. Figure 2(a) shows the opening area for the deposited Ag. In this process, the Ag material was heated to a high temperature, causing it to evaporate and subsequently condense onto the substrate, forming a thin film. The process was carefully handled to ensure that the thickness of the Ag layer was roughly 300 nm.

After the deposition process, a 5-second chlorination step was carried out using $FeCl_3$ to form the Ag/AgCl RE. This process involved the reaction between Ag and $FeCl_3$, forming AgCl on the surface of the Ag layer. The Ag/AgCl RE provides a stable potential for pH-sensing measurements. After forming Ag/AgCl, the area of Ag/AgCl was covered using Kapton tape, as shown in Figure 2(b), for deposited TiO_2.

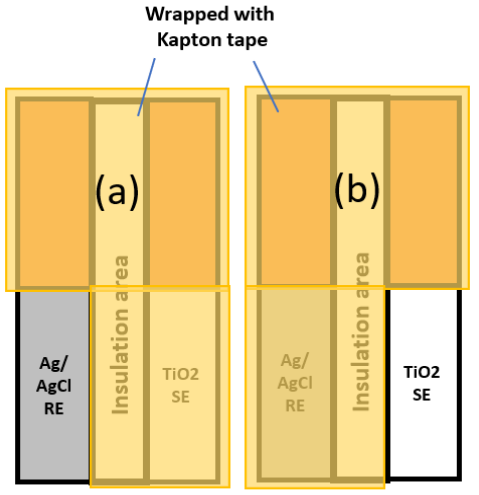

Figure 2. Schematic diagram during (a) Ag layer and (b) TiO_2 deposition process

Measurement Setup

Figure 3 illustrates the experimental arrangement employed for conducting EGFET measurements, comprising the integration of an IASE and TiO_2 SE with a commercialized RE connected with a semiconductor device analyzer (SDA). Furthermore, the commercialized RE was linked to SMU 3, while the TiO_2 SE was connected to the pin gate of a commercially available CD40007UBE

MOSFET, serving as the extended gate SE. This transistor was used as a readout to extract a potential change on the gate site

by converting it to drain current. This commercialized transistor can be assembled on a printed circuit board (Kwon et al., 2019).

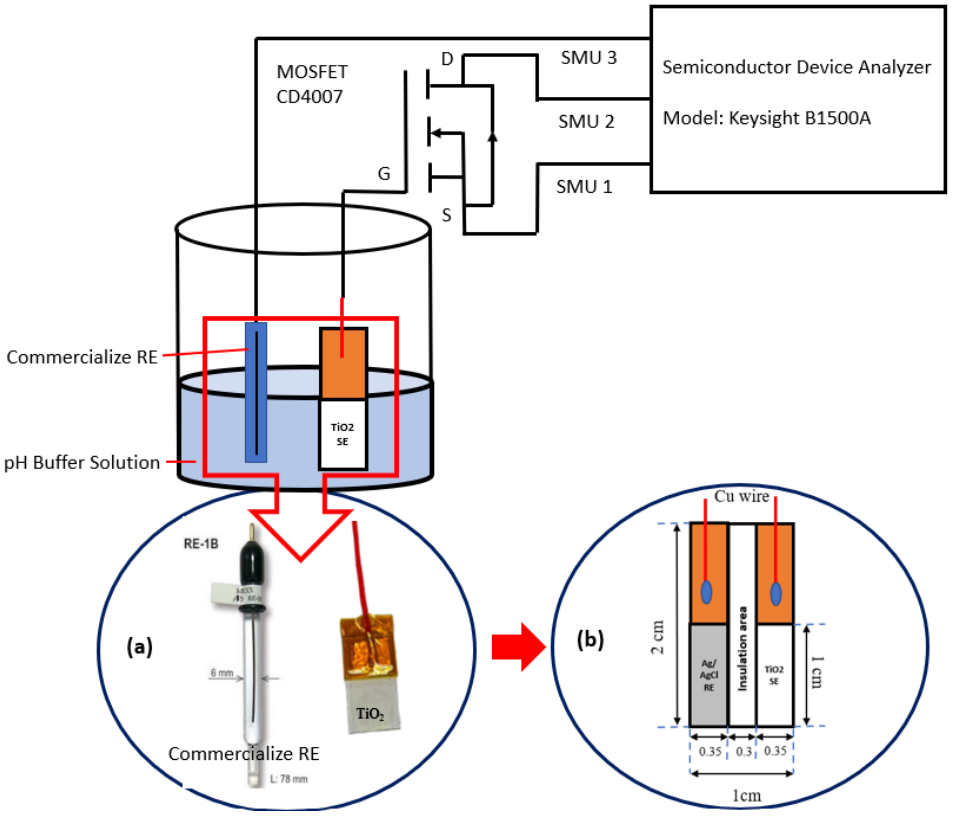

Figure 3. EGFET measurement setup (a) TiO_2 SE and commercialize RE (b) IASE

Various pH buffer solutions were employed to explore the sensor's response capabilities. The IASE was immersed in different pH buffer solutions, including those with 2, 4, 7, 10, and 12 pH values. The transfer characteristic (drain current, I_D versus reference voltage, V_{REF}) and the output characteristic (drain current, I_D versus drain-source voltage, V_{DS}) were obtained from these measurements. During transfer characteristic measurement, the V_D was set at 100 mV, and V_{REF} sweeps from 0 to 3 V. To assess the pH sensitivity performance of the fabricated IASE, a graph depicting the relationship between the drain current and the reference voltage was evaluated. The output voltage was extracted from the I_D versus V_{REF} curve as the obtained I_D of 100 µA corresponding to an applied reference voltage.

RESULTS AND DISCUSSION

Figures 4 to 8 show the transfer characteristics (left) and output voltage graphs (right) for fabricated IASE at room temperature, 30°C, 50°C, 70°C, and 100°C, respectively.

All transfer characteristic graphs exhibit similar patterns from the result obtained with the threshold voltage shifted from a rightward direction. As can be seen on the graph, by increasing the pH value from pH 2 to pH 12, the threshold voltage shifted from the left to the right direction due to a decrease in hydrogen ion concentration, which reduced the surface potential (Das et al., 2014). The sensitivity and linearity were recorded at 66.1 mV/pH and 0.9561 at room temperature deposition. As the deposition temperature increased to 30°C, the sensitivity and linearity were around 64.2 mV/pH and 0.9423, respectively. Further, the temperature was increased to 50°C, and the sensitivity increased to 67.3 mV/pH, but the linearity slightly decreased to 0.9211. The sensitivity and linearity were around 66 and 66.7 mV/pH and 0.9343 and 0.9287, respectively, for temperature deposition at 70°C and 100°C. This result investigates site binding theories to explain how the oxide surface of a gate electrode detects the pH. The surface of the metal oxide goes through a process that causes it to create hydroxyl groups when immersed in a solution. These hydroxyl groups In general, the oxide surface is composed of a hydroxyl group, OH-.

Thus, when the metal oxide surface comes into contact with a solution, the surface reaction could be protonated by acidic or deprotonated ions in an alkaline solution, thus leaving positively or negatively charged ions on the surface of the sensing electrodes can either donate or accept a proton as shown in Figure 9. The surface of the sensing membrane denoted Ti can be in three different forms: neutral (TiOH), negative (TiO^-), and positive ($TiOH_2^+$). The changes in the surface potential depend on the value of the pH buffer solution. At a lower pH (acidic), hydrogen ions concentration is high, where more positive charges accumulate near the extended gate (SE) and attract more electrons to the interface between the gate and the substrate, allowing current to flow from the source to drain. However, a higher pH (alkaline) indicates low hydrogen ions concentration; the decrease in positive charge near the gate causes the threshold voltage to shift positively. In other words, the voltage required to turn on the MOSFET is increased (Sabah et al., 2017). The dependency of threshold voltage on the pH value can be illustrated using Equation 1.

$$[H^+]_s = [H^+]_b \exp(-q\varphi_o/kT) \qquad [1]$$

Where the $[H^+]_s$ and $[H^+]_s$ are the bulk and the surface activity of the H^+ ions, q is the electron charge, φ_0 is the potential on the gate of the transistor, k is the Boltzmann constant, and T is the absolute temperature. It was discovered that a lower value of φ_0 leads to a lower output voltage based on Equation 1.

Table 1 presents a comparative analysis of the sensitivity and linearity values of the IASE and TiO_2 SE compared to a commercially available RE. The impact of increasing drying temperature on these parameters was examined. The findings indicate no significant alterations as the drying temperature was raised. The average sensitivity of the IASE

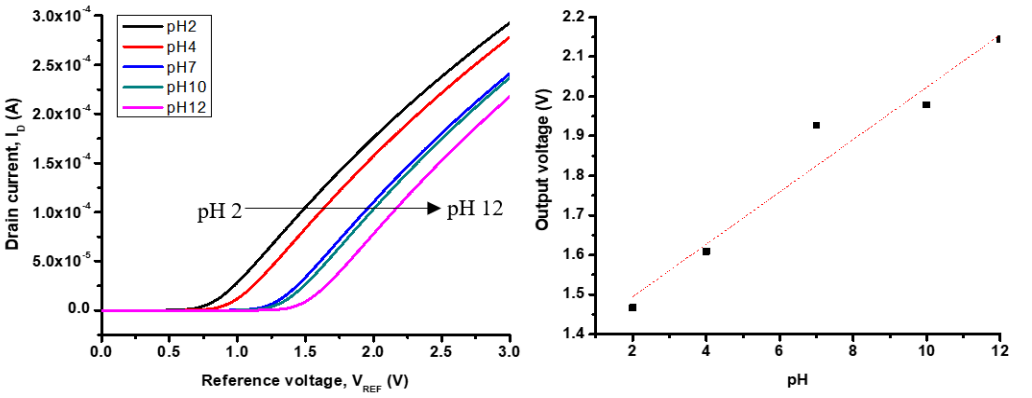

Figure 4. Transfer characteristic I_D versus V_{REF} and the graph of output voltage for IASE at room temperature

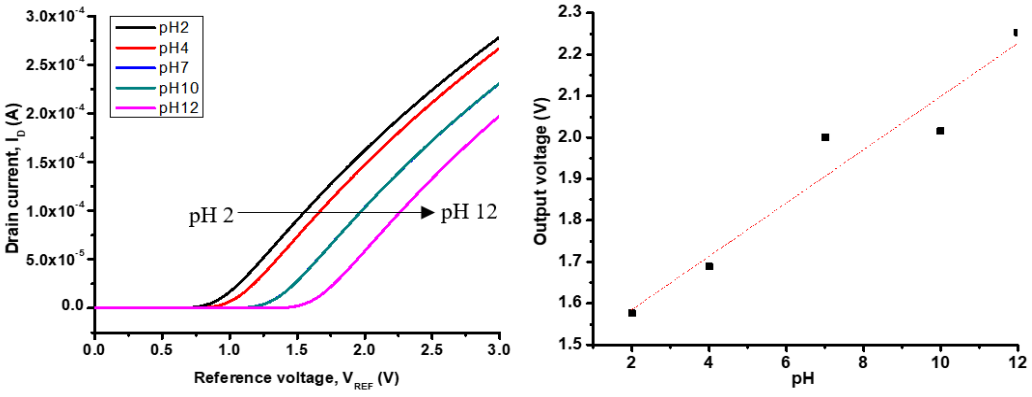

Figure 5. Transfer characteristic I_D versus V_{REF} and the graph of output voltage for IASE at 30°C

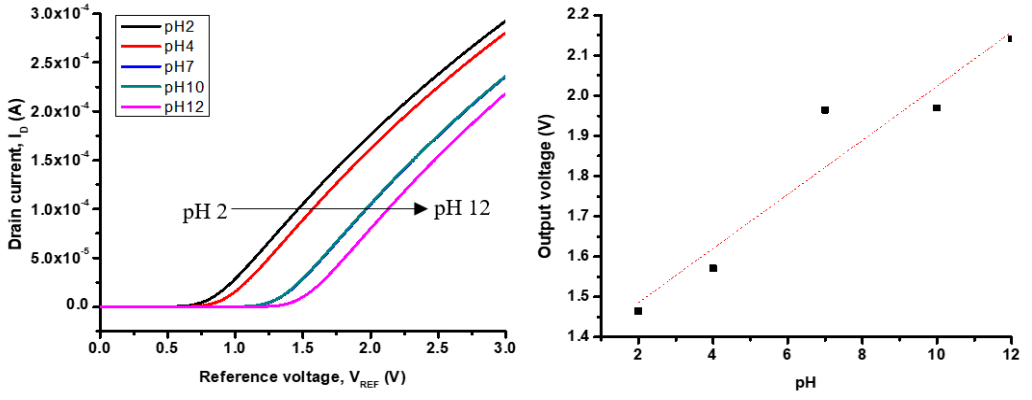

Figure 6. Transfer characteristic I_D versus V_{REF} and the graph of output voltage for IASE at 50°C

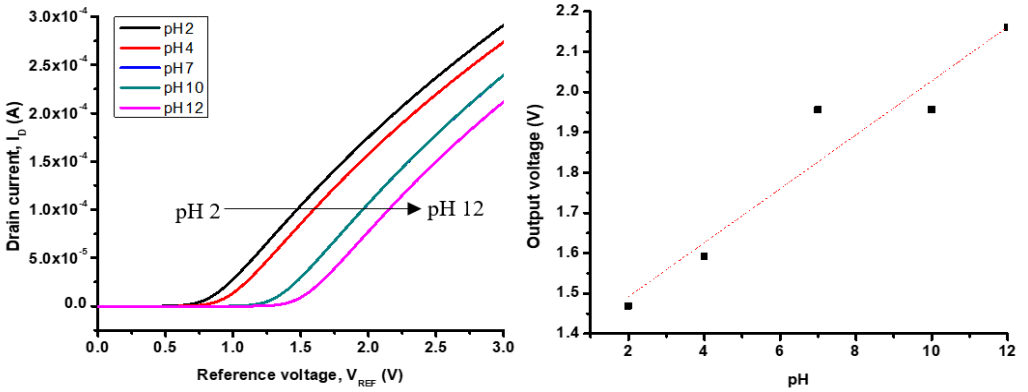

Figure 7. Transfer characteristic I_D versus V_{REF} and the graph of output voltage for IASE at 70°C

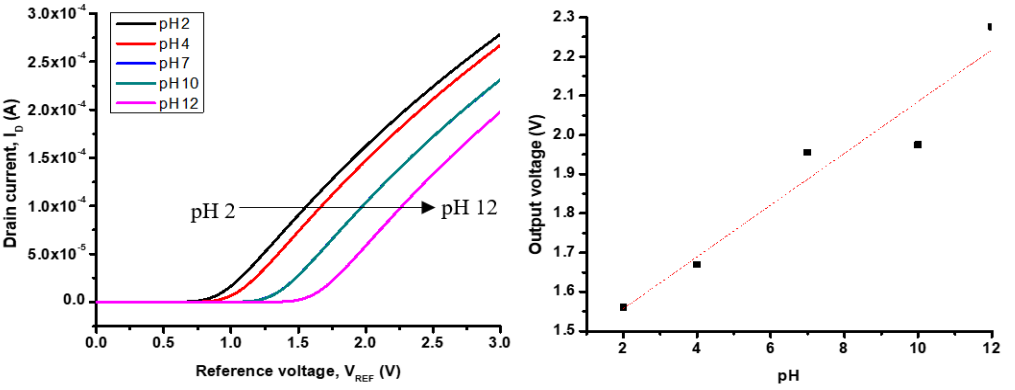

Figure 8. Transfer characteristic I_D versus V_{REF} and the graph of output voltage for IASE at 100°C

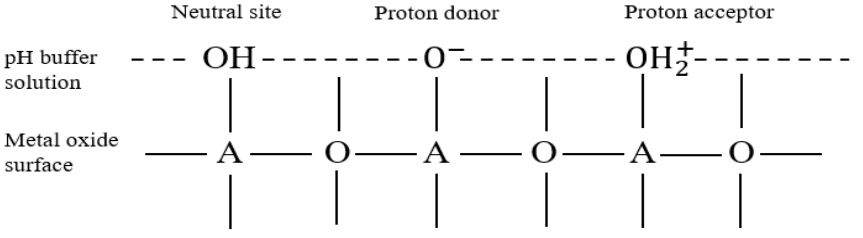

Figure 9. Schematic diagram of energy site binding

electrode was approximately 66.12 mV/pH, with the highest sensitivity of 67.3 mV/pH recorded at a drying temperature of 50°C. In the case of the TiO_2 SE and commercialized RE, the sensitivity increased from 46.3 mV/pH to 56.3 mV/pH as the drying temperature rose from room temperature to 70°C. Subsequently, it decreased to 52.7 mV/pH when

the drying temperature reached 100°C. Table 1 demonstrates that the TiO_2 SE and the commercialized RE exhibited superior linearity compared to the deposited IASE, albeit the disparity was still within an acceptable range.

Table 1
Comparison sensitivity and linearity value of IASE and TiO_2 SE

Temperature (°C)	IASE		SE+Commercialize RE	
	Sensitivity	Linearity	Sensitivity	Linearity
Room Temperature	66.1	0.9561	46.3	0.9565
30	64.2	0.9423	48.8	0.9935
50	67.3	0.9211	55.7	0.9999
70	66	0.9343	56.3	0.9994
100	66.7	0.9827	52.7	0.9947

The X-ray diffraction (XRD) pattern of TiO_2 thin films at various temperatures is shown in Figure 10. Based on the XRD analysis, it shows clearly notable peaks at 2θ values of approximately 26.24°, 35.41°, and 50.81° corresponding to the (101), (110), and (202) orientations, respectively. These peaks show similarity with several reported works (Abdullah et al., 2019; Bakri et al., 2017; Yao et al., 2014). The XRD peaks demonstrate that increasing temperature results in higher intensity of diffraction peaks. The intensity of XRD peaks reflects the amount and orientation of crystalline material in the thin film. The intensity of the TiO_2 redox peak increased with increased temperature, indicating a higher degree of crystallinity.

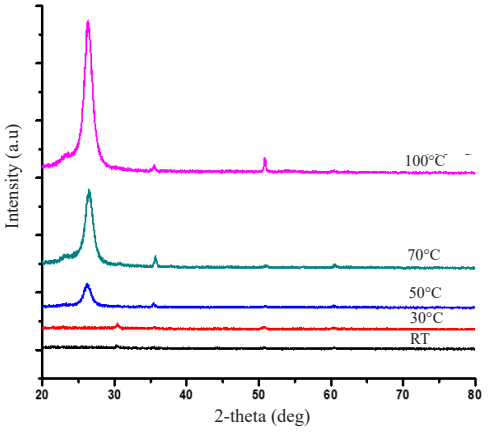

Figure 10. XRD pattern of TiO_2 thin films at different temperatures

Figure 11 shows the field effect scanning electron microscope (FESEM) images of TiO_2 thin film on an ITO-coated glass substrate at different deposition temperatures from RT to 100°C. As can be observed, the images at lower temperatures indicate a substrate covered in an uneven shape that contains a few gaps or cracks between TiO_2 particles. It shows that the TiO_2 particles are not sufficiently mobile to migrate and form a more compact structure during the first stages of heating. When the temperature is increased, a noticeable change can be seen in the FESEM images, in which fewer cracks were observed, and TiO_2 covered a larger surface area as the temperature increased

from 50 to 100°C. From Figure 11, the temperature also influences the grain size of TiO_2. As the temperature increases, the grain size becomes larger. Kamrosni et al. (2022) have discussed the effect of the annealing temperature of TiO_2 on the SEM images. This observation agrees with the hypothesis that higher temperatures promote denser coverage on the ITO-coated glass substrate by increasing the diffusion and aggregation of the TiO_2 particles.

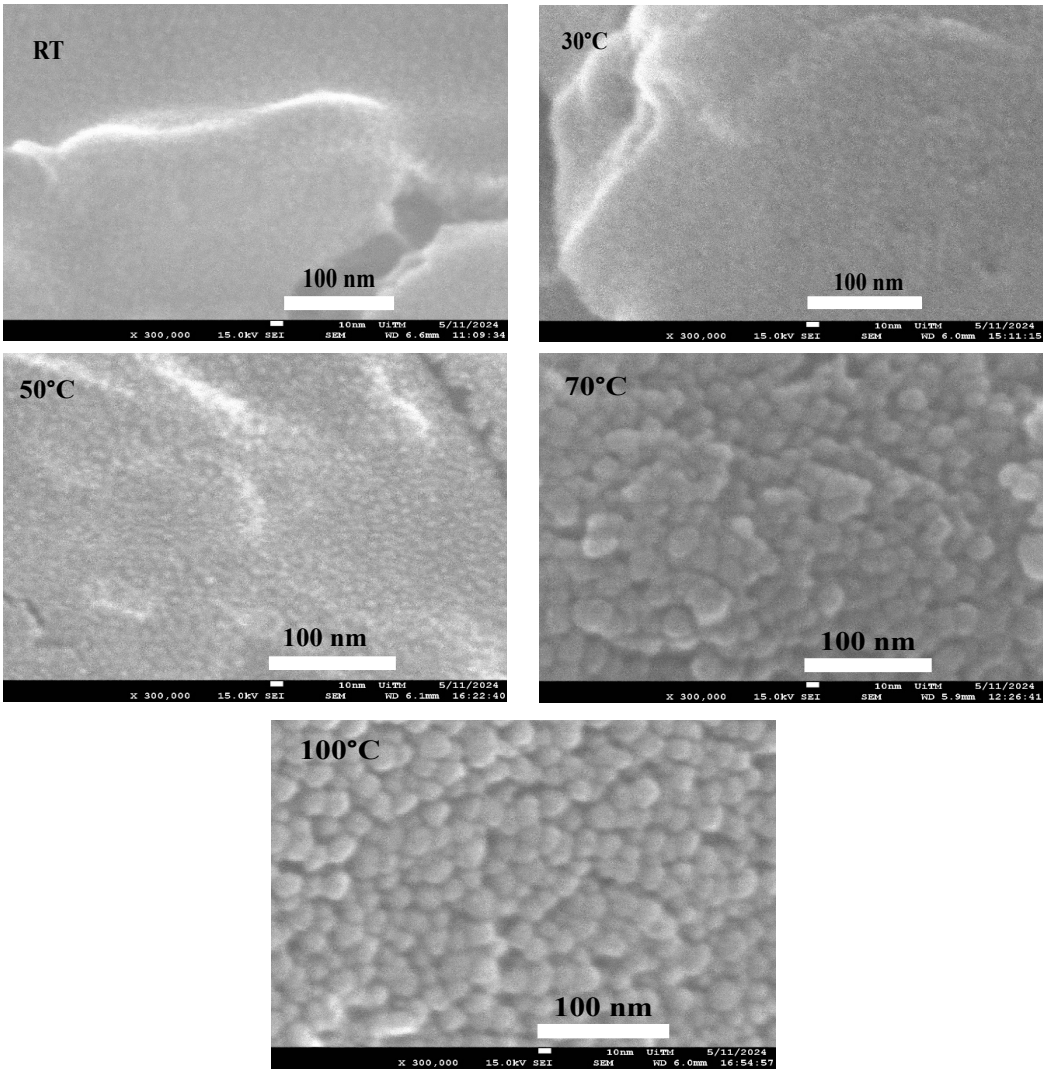

Figure 11. FESEM images of TiO_2 thin film on ITO-coated glass substrate at different temperatures (room temperature–100°C)

The connection between the FESEM observations and the XRD results depicted in Figure 10 is particularly intriguing. It is believable to suggest that the increased coverage

and combination of TiO_2 particles at higher temperatures, as seen in the SEM images, may be responsible for the structural changes reflected in the XRD data. Specifically, the XRD patterns may reveal shifts or alterations in the crystalline phases of the TiO_2 thin film as a consequence of the temperature-dependent structural evolution witnessed in the SEM images.

The energy dispersive x-ray (EDX) spectra of the TiO_2 thin film are depicted in Figure 12. Figure 10 displays the peaks representing the elements found in the sample. It was determined that titanium (Ti) and oxygen (O) were present in the sample. This peak's energy is associated with the Ti electron shells, which were found to be between 4.5 and 5.0 keV, and O, which was seen to be at roughly 0.5 keV. The table in the inset illustrates the percentages of each element's atomic weight as well as its relative weight. Ti has the highest weight percentage at 54.6%, followed by element O with 31.4%, and both come from the ITO substrate and TiO_2, respectively.

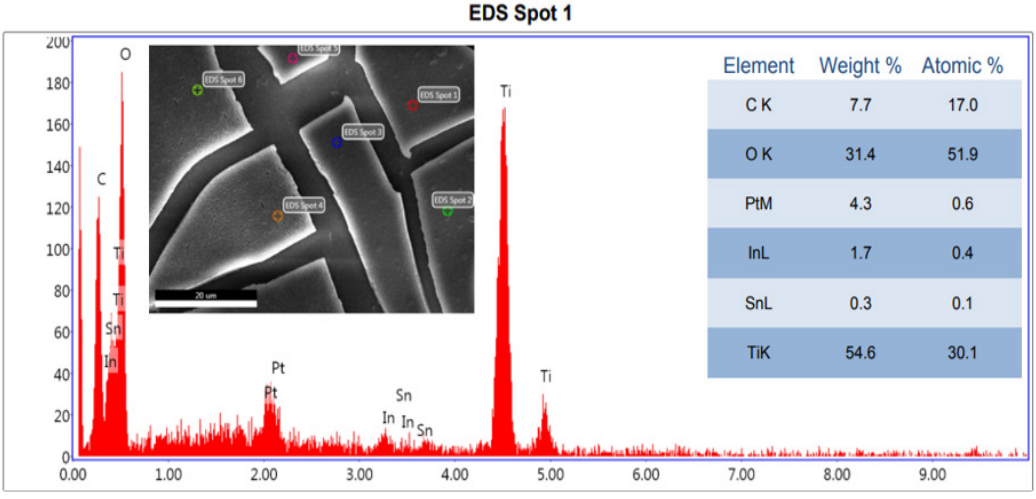

Figure 12. EDX spectra of TiO_2 thin film

CONCLUSION

In conclusion, the IASE-based TiO_2 SE and Ag/AgCl RE have been successfully fabricated on an ITO-coated glass substrate and are being compared TiO_2 SE with commercialized RE. The deposited IASE was more sensitive to pH measurement than TiO_2 SE with commercialized RE. However, the drying temperature does not show significant changes in IASE performance as the drying temperature increases. In addition, the TiO_2 SE and the commercialized RE's linearity were better than that of the deposited IASE. Although, the linearity of the IASE was still considered acceptable.

ACKNOWLEDGMENTS

The present study acknowledges the financial support the Ministry of Higher Education Malaysia provided through the Fundamental Research Grant Scheme [Project Code: FRGS/1/2021/TK0/UITM/02/50]. The authors would also like to thank the NANO Electronic Centre (NET) UiTM for their support.

REFERENCES

Abdullah, S. A., Sahdan, M. Z., Nafarizal, N., Saim, H., Cik Rohaida, C. H., & Adriyanto, F. (2019, July 24-25). *XRD and Raman spectroscopy study on the effects of post-annealing temperature of TiO_2 thin films.* [Paper presentation]. IEEE International Conference on Sensors and Nanotechnology, Penang, Malaysia. https://doi.org/10.1109/SENSORSNANO44414.2019.8940092

Bakri, A. S., Sahdan, M. Z., Adriyanto, F., Raship, N. A., Said, N. D. M., Abdullah, S. A., & Rahim, M. S. (2017). Effect of annealing temperature of titanium dioxide thin films on structural and electrical properties. *AIP Conference Proceedings*, *1788,* Article 030030. https://doi.org/10.1063/1.4968283

Beale, C., Altana, A., Hamacher, S., Yakushenko, A., Mayer, D., Wolfrum, B., & Offenhäusser, A. (2022). Inkjet-printed Ta_2O_5 on a flexible substrate for capacitive pH sensing at high ionic strength. *Sensors and Actuators B: Chemical*, *369*, Article 132250. https://doi.org/10.1016/j.snb.2022.132250

Bergveld, P. (1972). Development, operation, and application of the ion-sensitive field-effect transistor as a tool for electrophysiology. *IEEE Transactions on Biomedical Engineering*, *BME-19*(5), 342–351. https://doi.org/10.1109/TBME.1972.324137

Chalitangkoon, J., & Monvisade, P. (2021). Synthesis of chitosan-based polymeric dyes as colorimetric pH-sensing materials: Potential for food and biomedical applications. *Carbohydrate Polymers*, *260*, Article 117836. https://doi.org/10.1016/j.carbpol.2021.117836

Das, A., Ko, D. H., Chen, C. H., Chang, L. B., Lai, C. S., Chu, F. C., Chow, L., & Lin, R. M. (2014). Highly sensitive palladium oxide thin film extended gate FETs as pH sensor. *Sensors and Actuators, B: Chemical*, *205*, 199–205. https://doi.org/10.1016/j.snb.2014.08.057

Dave, D. P., & Chauhan, K. V. (2022). Synthesis of visible spectrum-active TiO_2 thin film induced by RF magnetron sputtering. *Materials Today: Proceedings*, *62*, 4254–4259. https://doi.org/10.1016/j.matpr.2022.04.755

Fathi, M., Babaei, A., & Rostami, H. (2022). Development and characterization of locust bean gum-Viola anthocyanin-graphene oxide ternary nanocomposite as an efficient pH indicator for food packaging application. *Food Packaging and Shelf Life*, *34*, Article 100934. https://doi.org/10.1016/j.fpsl.2022.100934

Gao, L., Liu, P., Liu, L., Li, S., Zhao, Y., Xie, J., & Xu, H. (2022). κ-carrageenan-based pH-sensing films incorporated with anthocyanins or/and betacyanins extracted from purple sweet potatoes and peels of dragon fruits. *Process Biochemistry, 121*, 463-480. https://doi.org/10.1016/j.procbio.2022.07.019

He, Y., Lu, L., Lin, Y., Li, R., Yuan, Y., Lu, X., Zou, Y., Zhou, W., Wang, Z., & Li, J. (2022). Intelligent pH-sensing film based on polyvinyl alcohol/cellulose nanocrystal with purple cabbage anthocyanins for visually monitoring shrimp freshness. *International Journal of Biological Macromolecules*, *218*, 900–908. https://doi.org/10.1016/j.ijbiomac.2022.07.194

Kamrosni, A. R., Suryani, C. H. D., Azliza, A., Mohd. Mustafa, A. B. A., Mohd. Arif Anuar, M. S., Norsuria, M., Chobpattana, V., Kaczmarek, L., Jez, B., & Nabialek, M. (2022). Microstructural studies of Ag/Tio_2 thin film; Effect of annealing temperature. *Archives of Metallurgy and Materials*, *67*(1), 241–245. https://doi.org/10.24425/amm.2022.137496

Khizir, H. A., & Abbas, T. A. H. (2022). Hydrothermal synthesis of TiO_2 nanorods as sensing membrane for extended-gate field-effect transistor (EGFET) pH sensing applications. *Sensors and Actuators A: Physical*, *333,* Article 113231. https://doi.org/10.1016/j.sna.2021.113231

Krishnan, S. G., Archana, P. S., Vidyadharan, B., Misnon, I. I., Vijayan, B. L., Nair, V. M., Gupta, A., & Jose, R. (2016). Modification of capacitive charge storage of TiO_2 with nickel doping. *Journal of Alloys and Compounds*, *684*, 328–334. https://doi.org/10.1016/j.jallcom.2016.05.183

Kwon, J., Yoo, Y. K., Lee, J. H., & Ahn, J. H. (2019). pH sensing characteristics of extended-gate field-effect transistor with Al_2O_3 layer . *Journal of Nanoscience and Nanotechnology*, *19*(10), 6682–6686. https://doi.org/10.1166/jnn.2019.17093

Manjakkal, L., Szwagierczak, D., & Dahiya, R. (2020). Metal oxides based electrochemical pH sensors: Current progress and future perspectives. *Progress in Materials Science*, *109*, Article 100635. https://doi.org/10.1016/j.pmatsci.2019.100635

Mokhtarifar, N., Goldschmidtboeing, F., & Woias, P. (2018, May 14-17). Low-cost EGFET-based pH-sensor using encapsulated ITO / PET-electrodes. *IEEE International Instrumentation and Measurement Technology Conference (I2MTC)*, Texas, USA. https://doi.org/10.1109/I2MTC.2018.8409571

Özdemir, A. O., Caglar, B., Çubuk, O., Coldur, F., Kuzucu, M., Guner, E. K., Doğan, B., Caglar, S., & Özdokur, K. V. (2022). Facile synthesis of TiO_2-coated cotton fabric and its versatile applications in photocatalysis, pH sensor and antibacterial activities. *Materials Chemistry and Physics*, *287*, Article 126342. https://doi.org/10.1016/j.matchemphys.2022.126342

Pal, B., Bakr, Z. H., Krishnan, S. G., Yusoff, M. M., & Jose, R. (2018). Large scale synthesis of 3D nanoflowers of SnO_2/TiO_2 composite via electrospinning with synergistic properties. *Materials Letters*, *225*, 117–121. https://doi.org/10.1016/j.matlet.2018.04.120

Palit, S., Singh, K., Lou, B. S., Her, J. L., Pang, S. T., & Pan, T. M. (2020). Ultrasensitive dopamine detection of indium-zinc oxide on PET flexible based extended-gate field-effect transistor. *Sensors and Actuators, B: Chemical*, *310*, Article 127850. https://doi.org/10.1016/j.snb.2020.127850

Pullano, S. A., Critello, C. D., Mahbub, I., Tasneem, N. T., Shamsir, S., Islam, S. K., Greco, M., & Fiorillo, A. S. (2018). EGFET-based sensors for bioanalytical applications: A review. *Sensors*, *18*(11), Article 4042. https://doi.org/10.3390/s18114042

Radha, E., Komaraiah, D., Sayanna, R., & Sivakumar, J. (2022). Influence of dysprosium ions on structural, optical, luminescence properties and photocatalytic ability of spin coated dysprosium ions doped TiO_2 thin films. *Thin Solid Films*, *761*, Article 139519. https://doi.org/10.1016/j.tsf.2022.139519

Ramakrishnappa, T., Sureshkumar, K., & Pandurangappa, M. (2020). Copper oxide impregnated glassy carbon spheres based electrochemical interface for nitrite/nitrate sensing. *Materials Chemistry and Physics*, *245*, Article 122744. https://doi.org/10.1016/j.matchemphys.2020.122744

Sabah, F. A., Ahmed, N. M., Hassan, Z., & Almessiere, M. A. (2017). Influences of substrate type on the pH sensitivity of CuS thin films EGFET prepared by spray pyrolysis deposition. *Materials Science in Semiconductor Processing*, *63*, Article 269–278. https://doi.org/10.1016/j.mssp.2017.02.032

Sadig, H. R., Cheng, L., & Xiang, T. F. (2019). Synthesis of tetra-metal oxide system based pH sensor via branched cathodic electrodeposition on different substrates. *Arabian Journal of Chemistry*, *12*(5), 610–620. https://doi.org/10.1016/j.arabjc.2018.10.010

Sharma, N., & Kumar, R. (2022). Effect of spin speed on the properties of TiO_2 thin films. *Materials Today: Proceedings*, *62*, 6615–6618. https://doi.org/10.1016/j.matpr.2022.04.614

Song, J., Lee, D., Oh, S., Kim, H. K., & Choi, S. (2023). Restacking-free crumpled anatase TiO_2 nanosheets synthesized by spray pyrolysis for high-performance Na-ion battery anodes. *Journal of Alloys and Compounds*, *941*, Article 169028. https://doi.org/10.1016/j.jallcom.2023.169028

Spiegel, J. V. D., Lauks, I., Chan, P., & Babic, D. (1983). The extended gate chemically sensitive field effect transistor as multi-species microprobe. *Sensors and Actuators*, *4*, 291–298. https://doi.org/10.1016/0250-6874(83)85035-5

Tayeb, A. M., Solyman, A. A. A., Hassan, M., & el-Ella, T. M. A. (2022). Modeling and simulation of dye-sensitized solar cell: Model verification for different semiconductors and dyes. *Alexandria Engineering Journal*, *61*(12), 9249–9260. https://doi.org/10.1016/j.aej.2022.02.057

Yang, K., Zhong, S., Zhou, X., Tang, S., Qiao, K., Ma, K., Song, L., Yue, H., & Liang, B. (2023). Controllable Al_2O_3 coating makes TiO_2 photocatalysts active under visible light by pulsed chemical vapor deposition. *Chemical Engineering Science*, *277*(24), Article 118792. https://doi.org/10.1016/j.ces.2023.118792

Yao, P. C., Lee, M. C., & Chiang, J. L. (2014, June 10-12). *Annealing effect of sol-gel TiO_2 thin film on pH-EGFET sensor*. [Paper presentation]. International Symposium on Computer, Consumer and Control, Taichung, Taiwan. https://doi.org/10.1109/IS3C.2014.157

Zamiri, G., Haseeb, A. S. M. A., Jagadish, P., Khalid, M., Kong, I., & Krishnan, S. G. (2022). Three-dimensional graphene-TiO_2-SnO_2ternary nanocomposites for high-performance asymmetric supercapacitors. *ACS Omega*, *7*(48), 43981–43991. https://doi.org/10.1021/acsomega.2c05343

Zulkefle, M. A., Herman, S. H., Rahman, R. A., Yusof, K. A., Rosli, A. B., Abdullah, W. F. H., & Zulkifli, Z. (2021). Evaluation on the egfet ph sensing performance of sol-gel spin coated titanium dioxide thin film. *Jurnal Teknologi*, *83*(4), 119–125. https://doi.org/10.11113/jurnalteknologi.v83.16313

Zou, Y., Sun, Y., Shi, W., Wan, B., & Zhang, H. (2023). Dual-functional shikonin-loaded quaternized chitosan/polycaprolactone nanofibrous film with pH-sensing for active and intelligent food packaging. *Food Chemistry*, *399*, Article 133962. https://doi.org/10.1016/j.foodchem.2022.133962